Am J Transl Res 2022;14(5):2910-2925
www.ajtr.org /ISSN:1943-8141/AJTR0141633

Original Article

Hydrogel modification of 3D printing hybrid tracheal scaffold to construct an orthotopic transplantation

Shu Pan[1*], Ziqing Shen[1*], Tian Xia[1], Ziyin Pan[2,3,4], Yibo Dan[2,3,4], Jianfeng Li[2,3,4], Hongcan Shi[2,3,4]

[1]Department of Thoracic Surgery, The First Affiliated Hospital of Soochow University, Suzhou 215000, Jiangsu, China; [2]Clinical Medical College, Yangzhou University, Yangzhou 225000, Jiangsu, China; [3]Institute of Translational Medicine, Medical College, Yangzhou University, Yangzhou 225000, Jiangsu, China; [4]Jiangsu Key Laboratory of Integrated Traditional Chinese and Western Medicine for Prevention and Treatment of Senile Diseases, Yangzhou University, Yangzhou 225000, Jiangsu, China. [*]Equal contributors.

Received January 9, 2022; Accepted April 6, 2022; Epub May 15, 2022; Published May 30, 2022

Abstract: Objective: To evaluate the biological properties of modified 3D printing scaffold (PTS) and applied the hybrid graft for *in situ* transplantation. Methods: PTS was prepared via 3D printing and modified by Pluronic F-127. Biocompatibility of the scaffold was examined *in vitro* to ascertain its benefit in attachment and proliferation of bone marrow mesenchymal stem cells (BMSCs). Moreover, a hybrid trachea was constructed by combining the modified PTS with decellularized matrix. Finally, two animal models of *in situ* transplantation were established, one for repairing tracheal local window-shape defects and the other for tracheal segmental replacement. Results: The rough surface and chemical elements of the scaffold were improved after modification by Pluronic F-127. Results of BMSCs inoculation showed that the modified scaffold was beneficial to attachment and proliferation. The epithelial cells were seen crawling on and attaching to the patch, 30 days following prothetic surgery of the local tracheal defects. Furthermore, the advantages of the modified PTS and decellularized matrix were combined to generate a hybrid graft, which was subsequently applied to a tracheal segmental replacement model. Conclusion: Pluronic F-127-based modification generated a PTS with excellent biocompatibility. The modified scaffold has great potential in development of future therapies for tracheal replacement and reconstruction.

Keywords: 3D printing scaffold, hydrogel carrier, surface modification, tissue engineering tracheal transplantation

Introduction

Research on tracheal substitutes has been going on for more than a century, with scaffolds ranging from allogeneic tracheal substitutes or synthetic materials, such as metal to current autoimmunity-deprived or biomimetic tracheal substitutes [1]. The choice of scaffolds is so significant that it directly affects success of the entire tissue engineering project. Scholars have been striving to identify an ideal tracheal scaffold that can provide an optimal environment for cell transplantation, growth and differentiation [2]. In recent years, the preparation process of scaffolds has also made great progress, which is also proved by the emergence of a number of new technologies such as electrospinning technology and 3D printing [3]. Moreover, the scaffold structure has become more complex (semi-annular, mesh or bellows, among others). Although a variety of bioactive biomimetic scaffolds from either natural or synthetic sources have been applied *in vitro*, animal models or clinical cases, an optimal scaffold for these applications remains uncertain [4]. The tracheal matrix, comprising just one single material, cannot meet the requirements of clinical tracheal substitutes which turn out to be biomimetic, individualized-manufacturing and have functional diversities [5]. Some researchers have already made some attempts to identify superior scaffolds, such as combining natural with synthetic materials, polymers and memory alloy materials [6]. Despite some progress in these attempts, there is still a long way to go before the most ideal tracheal substitutes are created.

Previous researche has proved that using a traditional single scaffold alone presents several limitations. Therefore, combining the hybrid graft with each scaffold's respective advantages may be a feasible approach to improve the physiological environment's recovery and functional replacement of reconstructed airway. Previous studies have also demonstrated that the ECM structure, biocompatibility and low immune rejection can still be retained using modified detergent-enzymatic method (DEM) decellularization [7]. For example, 20% concentration of Pluronic F-127 can be used as a suitable carrier to support proliferation and differentiation of BMSCs, and this enhances effect of the capsuling growth factor [8]. In this study, the properties of a PTS modified by Pluronic F-127 were evaluated firstly, then combined the modified PTS with a decellularized matrix to construct a hybrid tracheal graft. Two animal models were established, one for repair of tracheal partial window-shape defect and the other for tracheal segmental defect replacement. Results of *in situ* transplantations were evaluated and compared.

Materials

Ethics statement

All animals received humane care in accordance with the "Guide for Care of Laboratory Animals" formulated by the National Ministry of Science (IACUC No. SYXK2016-0041) and was approved by The First Affiliated Hospital of Soochow University (ethical approval No. 2020-275) and confirmed to the principles outlined in the Declaration of Helsinki. The experimental animals were treated humanely, and all efforts were made to ease their discomfort.

Animals

Male or female New Zealand rabbits, aged under two months and weighing between 0.5 and 1.0 kg, were purchased from the Experimental Animal Center of Yangzhou University. Their bone marrows were aspirated and the rabbits fed until they were three months old for the subsequent *in situ* transplantation.

Seed cells

A sterilized medullo-puncture needle was vertically inserted into the tibial plateau of the rabbit, a syringe containing 0.5 ml heparin connected to draw approximately 1 ml of the bone marrow, and the heparin removed by centrifugation. BMSCs were obtained and purified using whole bone marrow adherent culture method. Cell passage was performed according to our previous protocol [7], and fourth-generation BMSCs planted on a 0.5 cm×0.5 cm trachea. The cells were soaked in 75% ethanol for 1 h, sterilized using ultraviolet irradiation for 2 h, then a 50 μl suspension of 3×10^4 BMSCs inoculated on each group in well plates. The cultures were incubated for 4 h, after which initial plates were removed and replaced, followed by addition of 50 μl of DMEM/F12 basal medium supplemented with 10% FBS to each well. The culture medium was changed after every 48 h, after which all the BMSCs were postoperatively transplanted into the same New Zealand rabbits where the stem cells had been obtained.

Scaffolds preparation and groups

(1) To evaluate the effect of modified PTS, three groups (n=6 in each group) were set up as follows; Group A1, B1 and C1 corresponds to native tracheas, unmodified PTS and scaffolds modified with Pluronic F-127 hydrogel, respectively. (2) The experiment for airway local window-shape defect repairment was divided into three groups (n=6 in each group, and four additional cases were set in the group C2 to evaluate the long-term effects). Specifically, Group A2 comprised autologous native tracheal repairment, B2 used a patch modified with Pluronic F-127, whereas C2 utilized a patch modified with Pluronic F-127 hydrogel carrying growth factor (TGF-*β)* and stem cells (200 μl of culture medium containing 2×10^5 cells). (3) The rabbit tracheal segmental defect replacement model comprised four groups (n=6 per group, with four additional cases set in group D3 to represent evaluations of long-term effects). Here, Group A3 was prepared by modified DEM method, which based on our previous protocol [7]. Group B3 was based on Group A3, except that it was cross-linked with 1% concentration of genipin in PBS solution at 37°C for 1 h. On the other hand, Group C3 involved use of a tubular PTS modified by Pluronic F-127. Whereas the group D3 was based on group B3, but included an additionally suturing of the "C"-shape PTS onto the "C"-shape cartilagi-

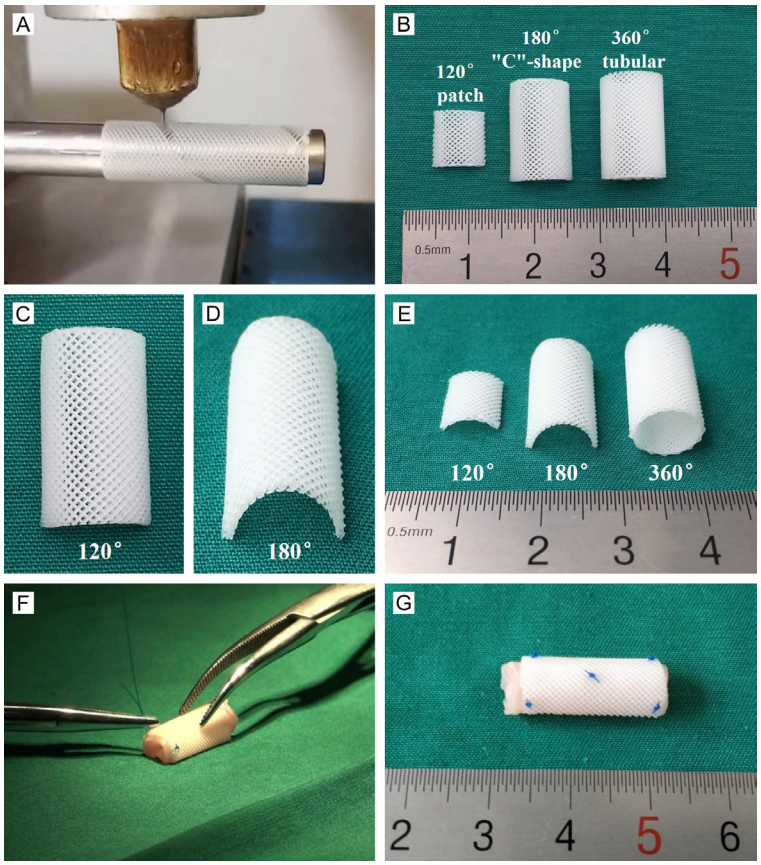

Figure 1. The process for creating porous tracheal scaffolds by 3D-printing technology (A: Tubular porous structure). The different rotation angles produced different printing structures, which were displayed from (B-E). The stitching (F) and forming (G) of hybrid scaffold.

nous matrix. All surgical sutures were 4-0 Proline, which was later used to establish the segmental tracheal defect animal model (**Figure 1F**, **1G**).

Methods

Preparation of the PTS and its surface modification

The polycaprolactone (PCL) was used as the material, the printing temperature at was maintained at 90°C, while the printer's nozzle was located directly on the rotating shaft at a speed of 5 mm/s. The printing nozzle moved back and forth, in the direction of the rotating shaft, and the thickness of each printed-layer was kept at 0.1 mm, altogether making six layers. The difference between the patch (120°), "C"-shape (180°) external and tubular (360°) scaffolds was that the rotation axes on their bases rolled at different angles. The printed products are shown in **Figure 1**, which made by the nozzle moved back and forth on the rotating shaft to produce various forms of scaffolds. Then the scaffolds were soaked with 200 nm pore sizes in 20% Pluronic F-127 solution for surface modification at 4°C overnight, followed by incubating at room temperature for five days. The dehydration process was completed after polymerization and condensation by reacting with the ester group on the surface of the material.

EDS analysis and SEM observation

Proportions of elements on the surface of the scaffold were analyzed using Energy dispersive spectrometer (EDS, since the PCL was fatty-soluble with a low melting point, care was taken not to use ethyl acetate and pure amyl ester. Similarly, it was not suitable to use a CO_2 dryer). The PTS was immersed in a 2.5% glutaraldehyde solution for 24 h, rinsed in PBS, dehydrated in ethanol, and finally vacuum-dried and sprayed with gold. The specimens were observed under Scanning electron microscope (SEM, S-4800) at different magnifications, and photographs taken.

Biocompatibility assessment

Preparation of scaffolds for sterilization: Each scaffold was trimmed into patches measuring 0.5 cm×0.5 cm, and washed repeatedly with PBS containing 1% AA, prior to cell inoculation. The PCL was not treated via high-pressure and high-temperature steam sterilization, owing to its low melting point. Therefore, the patches were submerged in 75% analytical ethanol for 30 min, then washed them with sterile PBS (2-3 times), before exposing each side of the materials to ultraviolet irradiation for 1 h. After completing every step, all the patches were moved into new 24-well plates for further use.

BMSCs vaccination and qualitative analysis of attachment: A 50 μl suspension of 4th generation BMSCs was slowly dropped onto the steril-

ized PCL patch (to ensure that the patch was just submerged) in 24-well plates, at a density of 3×10^4 cells/piece and incubated for an additional 4 h. Thereafter 50 μl of DMEM-F12 medium supplemented with 10% fetal bovine serum was continuously added to each well. The microstructures of samples were observed under SEM after 48 h of co-culture. The medium was changed every 48 h, for a period of one week. BMSCs attachment and proliferation conditions were evaluated after 1, 3, 5 and 7 days.

Analysis of cell proliferation and attachment: Medium surrounding the scaffold was aseptically aspirated, 100 μl of CCK-8 working solution (dilution ratio: 1:10) slowly added onto the scaffold surface of each sample under dark conditions, followed by incubation for 2 h. Next, 50 μl of the supernatant was transferred into a new 96-well plate and sample OD450 was measured using microplate reader to quantify proliferative and attachment effects of cells on each tissue.

Detection of contact cytotoxicity around scaffolds: The scaffolds were trimmed into 0.5 cm×0.5 cm pieces, under aseptic conditions, then attached to the 24-well plate's bottom with the outer side of the scaffold facing upwards. Surplus PBS surrounding scaffolds was removed. The scaffold was dyed in a sterile environment for 2 h, then DMEM/F12 medium supplemented with 10% FBS slowly dropped around its scaffold pieces. The well plates were incubated at 37°C, and 5% CO_2 saturation humidity for 24 h, and the medium aspirated out. Then the 4^{th}-generation BMSCs suspensions (containing 1×10^4) inoculated around the tissue pieces. The cell-scaffold complex was incubated for 48 h, and the adherent cells around it stained with Giemsa pigment dye. The BMSCs nucleus appeared blue-purple or purple-red, whereas the cytoplasm stained pink. Similarly, immunofluorescence was used to stain the nuclei of normal and apoptotic cells. The phenomenon can be explained by the fact that the dye passed through the cell membrane of living cells and finally combined with the cell nucleus. Notably, the nucleus appears green after fluorescent excitation (wavelength of 510 nm). The microscope was used to visualize cell attachment pattern around the scaffold and assess the contact toxicity.

Establishment of a rabbit model for tracheal partial window-shape defect repairment

Surgical procedure: Adult New Zealand rabbits (3-4 months old) were selected as recipients, while preparation of scaffolds was as previously described in section 3.3.1. The rabbits were given an intramuscular injection comprising xylazine hydrochloride at the dose of 0.15 ml/kg. A midline sternotomy was performed in the rabbit's neck, to dissociate the fascia and neck muscles, dissect the tissue around the trachea layer by layer, and retain as much fascia as possible. The window-shape defect was "opened" (size: 1 cm×0.8 cm), 2 cm away from the distal end of the first cartilage ring. The first stitch was pressed on the opposite side during anastomosis. To reduce the knots, a continuous suture method was adopted and tied out of the lumen. After suturing, the hydrogel carrier was smeared with ingredients of BMSCs (1.5×10^5/300 μl) and TGF-β1 (a final concentration of 200 ng/ml) on the outer surface of the scaffolds of group C2. Thereafter, the fascias and muscular bonds around the trachea were stretched during the operation regain and sutured them tightly around the patch. Finally, the fascial tissues and the skin incision were closed via the intermittent suturing method. To prevent infections, during the first week after surgery, the animals were maintained on a daily intramuscular injection of penicillin (5×10^4 U/kg). All transplantation groups were not treated with any immunosuppressive agents.

Analysis of postoperative survival status and specimen harvesting: The animals' general vital signs and activities were monitored and recorded, including body weight and symptoms such as wheezing, cyanosis, and nasal agitation. The animals were also given timely airway management, postoperative nutrition and anti-infection treatment. After 30 days, the animals were euthanized and specimens harvested.

Fiberoptic bronchoscopy and analysis of routine staining: The animals were injected with 0.15 ml/kg xylazine hydrochloride intramuscularly, on the 30^{th} day after operation (POD), as previously mentioned. Their airway and repair sites were then observed and photographed under fiberoptic bronchoscopy. The animals were sacrificed, by aeroembolism through marginal ear veins, to obtain a grafted matrix. The

collected specimens were fixed in 10% formalin (pH=7.4) at room temperature for 24 h, and embeded in paraffin, and then sectioned to 4 μm thickness using a microtome. The sections were stained as follows: the paraffin block was dewaxed twice in xylene for 10 min each time, then hydrated in ethanol from high to low concentration (8 min each time), then rinsed in distilled water for 1 min. They were then stained in Hematoxylin & eosin solution. The specimens were dehydrated in gradient ethanol, soaked twice in xylene and mounted on slides. The structural architecture of the tracheal repair sites, as well as the condition of the crawling epithelial lining, and infiltration of inflammatory cells were observed under the microscope.

Analysis of differentiation state of epithelial and stem cells: The epithelial cells' creeping condition and the differentiation effects of stem cells on the patch were analyzed via immunohistochemical (IHC) staining. Specifically, Cytokeratin-18 (CK-18) and type-II collagen antibodies (at a dilution ratio of CK-18 and Type-II collagen mixed in the primary antibody was 1:200) were used. The immunohistochemically-stained tissue sections were subjected to sub-regional structural morphology analysis. Briefly, the cross section of the trachea was divided into the outer part of the trachea (the area out of cartilage rings), cartilage matrix (the area between the tracheal rings and the lamina propria of the tracheal mucosa), and the section inside the lumen (the area excluding the submucosa inside the cartilage rings), and cell patterns and tissue structures of the same region compared.

Establishment of a rabbit tracheal segmental defect model

Surgical procedure: The adult New Zealand rabbits were selected as recipients, and prepared scaffolds as described in section 3.3.1. Cross-linking of genipin in group B3 and D3 was performed as described in our previous paper [9]. Briefly, the decellularized tracheal matrix was immersed in PBS solution, comprising 1% genipin, and cross-linked for 1 h at 37°C. In group D3, the PTS was sutured to the cross-linked decellularized matrix at the four corners and center, just before surgery, as shown in **Figure 8A**, **8B**.

The similar anesthesia and tracheal anatomy procedures were adopted, as described in section 3.4.1, made an incision 2 cm away from the distal end of the first tracheal cartilage ring and suspended the broken trachea with a silk thread. The excised section was about 2 cm in length, and care was taken to protect the distal trachea from postoperative atelectasis and infection. The anastomosis was performed from the posterior wall, with the first needle inserted at the interface of the tracheal membrane and the cartilage. A continuous tension suturing method was adopted to avoid skin tearing, and also sutured the cartilage portion in the same way, with the needle spacing adjusted according to the size of the incision. The knots were left out of the tracheal lumen, while subsequent treatments were as previously described in section 3.4.1.

Analysis of postoperative survival and specimen harvesting: The process was the same as that described in section 3.4.2. Animals in groups A3, B3, and C3 had postoperative complications, hence could not survive for 30 days. Therefore, they were euthanized and specimens harvested in time, upon appearance of symptoms such as wheezing and cyanosis.

Analysis of postoperative staining: The conventional staining was similar to that described in section 3.4.3. The analysis of the crawling epithelium was performed via fiberoptic bronchoscopy and IHC staining as described in section 3.4.4.

Statistical analysis

All data were analyzed using SPSS 20.0 statistical software, and presented as means ± standard deviations (SD) of the means. Comparisons between two groups were performed using a student's *t*-test whereas those among three or more groups were analyzed using analysis of variance (ANOVA). Data followed by $P< 0.05$ were considered statistically significant.

Results

Evaluation of the modification effect on the surface of PTS

The EDS results showed that the peak of element "C" value decreased after modification (**Figure 2A**, **2B**). Notably, the statistically signifi-

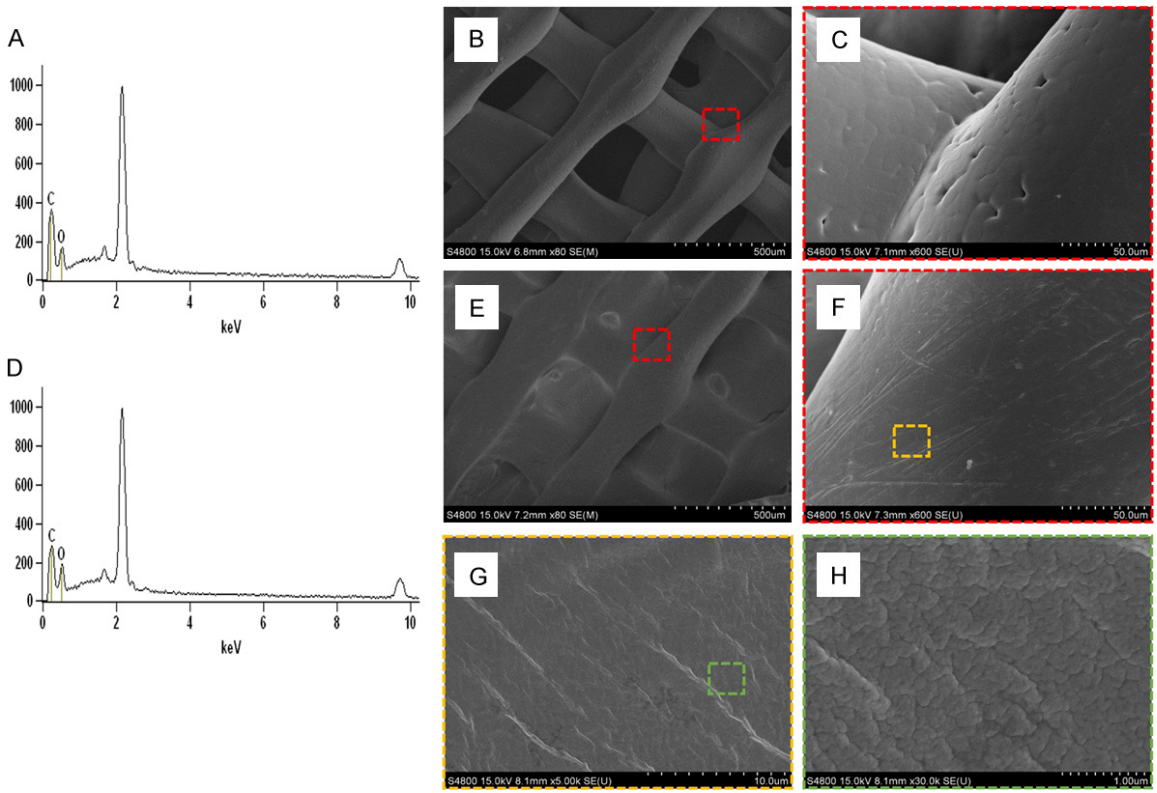

Figure 2. The EDS analysis of the composition ratio of each element on the surface of the scaffold (A: Unmodified scaffold, D: Modified scaffold). The results of SEM observation (B, C: Unmodified PCL scaffolds. E, F: Modified PCL scaffolds. G, H: Appearance of the gel at high magnification. Magnification: B, E: ×80, F: ×600, G: ×5000, H: ×30,000).

cant differences were found between the mass ratios of "C" and "O" after modification ($P<0.05$, *Student's t-test*), which was (54.72±0.92): (45.28±0.92) before modification, and (50.50±0.46): (49.50±0.46) after Pluronic F-127's modification. This result was also consistent with the chemical formula of the two scaffolds: the molecular formula of PCL is $(C_6H_{10}O_2)n$, while Pluronic F-127 is $HO\cdot(C_2H_4O)m\cdot(C_3H_6O)n\cdot H$. According to the molecular formula, the PCL scaffold has a larger "C" element mass than Pluronic F-127. Overall, these results affirmed the effectiveness of the modification scheme designed in this experiment.

SEM revealed that the surface of the unmodified PCL scaffold was rough, and had numerous dents (**Figure 2B**, **2C**). Modification with 20% Pluronic F-127 allowed filling of the pores and gaps with a thin layer of gel (**Figure 2E**). At high magnification, the scaffold appeared smoother and denser than before, while the dents almost disappeared (**Figure 2F**). Specifically, higher magnification enabled observation of ultra-structure of the gel, which was also arrayed in orderly directions (**Figure 2G**, **2H**).

Biocompatibility properties of the scaffolds and BMSCs

Appearance of cell attachment under SEM: SEM revealed that the cell attachment and growth were in good condition 48 h after inoculating BMSCs on the scaffolds across the three groups. Specifically, underlying cells appeared spindle-shaped, while those on top changed into bead-like shapes, and were distributed in clusters. Stem cells on the surface of the native trachea appeared cobblestone-like (**Figure 3A**), while the interstices of the PTS were filled with stem cells (**Figure 3E**, **3I**). At high magnification, stem cells across each group appeared to be in full shape and held out pseudopods. This phenomenon indicated that host cells migrated well on the surface of the scaffold (**Figure 3B**, **3F** and **3J**).

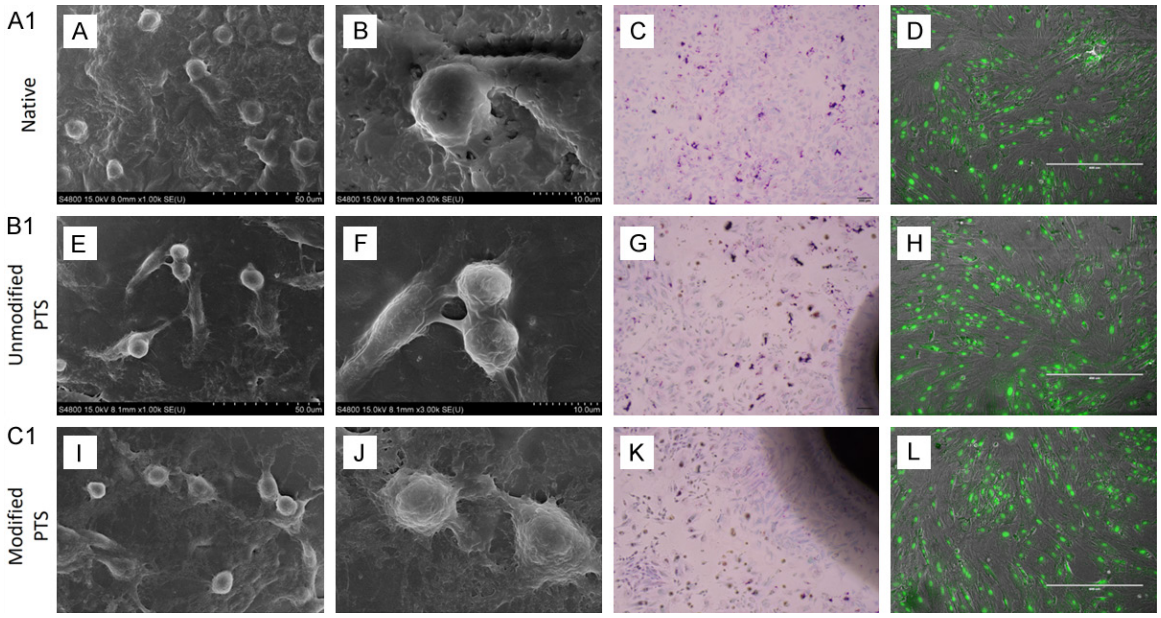

Figure 3. The cell appearance on the scaffold of each group for 48 h after inoculation. From top to bottom: A1, B1, C1 (Magnification: A, E and I: ×1,000; B, F and J: ×3,000). The appearance of stained cells following their inoculation around the scaffold. (Magnification: C, G and K: ×40; D, H and L: ×100).

Table 1. OD_{450} values of BMSCs inoculated on scaffolds across the three groups

	Native trachea	PCL	PCL after modification
1 d	0.080±0.002	0.091±0.005	0.089±0.013[a,b]
3 d	0.134±0.006	0.131±0.020	0.186±0.026[a,b]
5 d	0.421±0.014	0.444±0.011	0.492±0.031[a,b]
7 d	0.417±0.015	0.438±0.012	0.465±0.018[a,b]

Data shown are means ± SD after ANOVA, [a]P<0.05 comparison with native trachea group, [b]P<0.05 comparison with the pure PCL scaffold group.

Cell proliferation: The CCK-8 test was used to assess cell proliferation, and then we analyzed OD values across each group. Results showed that cells continued to proliferate from day 1 to 5, with cell number at day 5 found to be more than 4 times those at day 1 (**Table 1**). Notably, the number significantly reduced at day 7, possibly due to contact inhibition. Based on these results, it is evident that the modified PTS exerts significant benefits to attachment and proliferation of BMSCs (P< 0.05, by ANOVA). This property is attributed to the gel's loose structure as observed under high magnification electron microscopy (**Figure 2H**).

Contact toxicity of stem cells surrounding scaffolds: Giemsa staining revealed that normally adherent cells had a fusiform shape. Their nuclei appeared purple or violet, whereas their cytoplasms stained light purple. BMSCs around the tissue collected from Group A1 grew well (**Figure 3C**), with fluorescence showing that they appeared as marked clustered cell colonies (**Figure 3D**). Specimens from group B2 appeared as a small number of round or irregularly-shaped cells (most of which were suspended or had poor vitality, **Figure 3G**), whereas stem cells in group C1 were slightly sparsely distributed compared to those in group A1 (**Figure 3K**). However, fluorescent staining showed that cells from the two groups (A1 and C1) were both scattered in the similar shape like cords and their nuclei were clearly colored (**Figure 3H**, **3L**).

Establishment of a rabbit model for tracheal partial window-shape defect repairmen

Intraoperative anastomosis, postoperative survival rates and specimen harvesting: The suture-suspended method was used to preserve the anterior-cervical fascia and muscular system. Suturing of individuals in group A2 was completed immediately after opening the window-shape defect, while in group B2, it was necessary to reinforce the surrounding fascia and muscle at the site of anastomosis owing to the scaffold's porous structure. Oth-

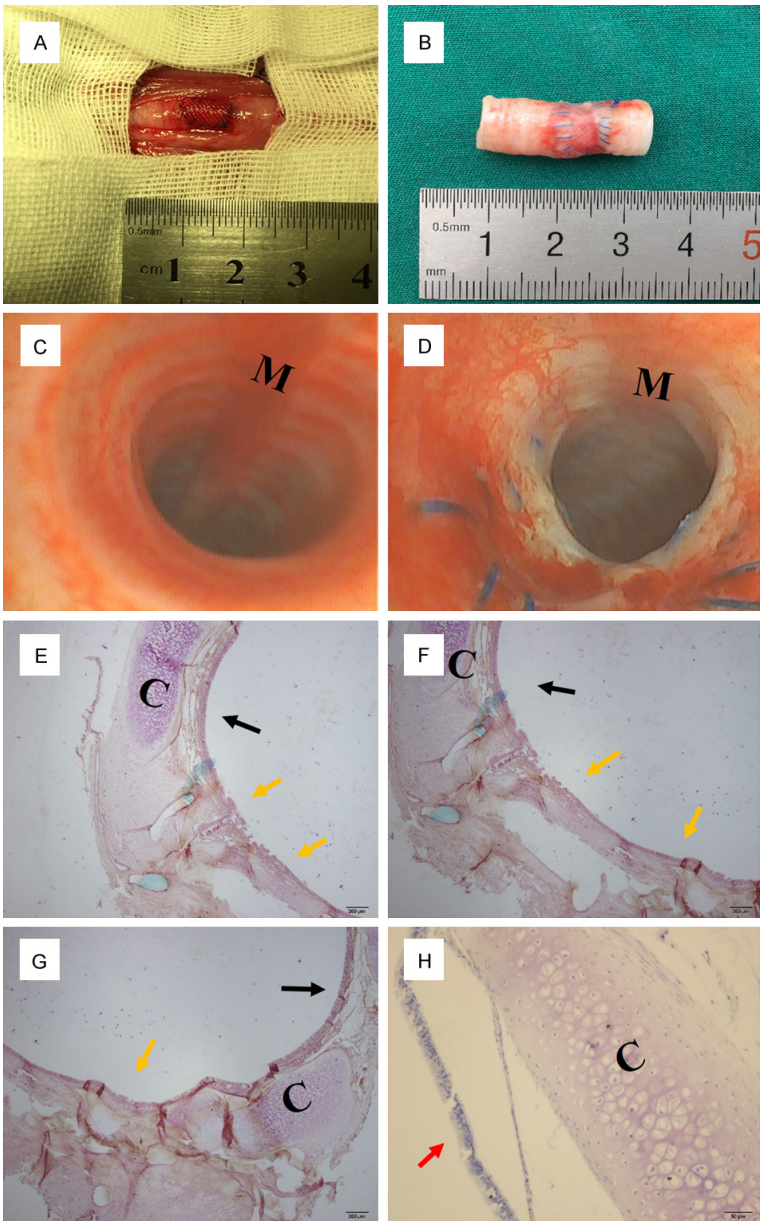

Figure 4. Intraoperative conditions across in group C2 (A: The suturing was done), and the representative photographs of harvested specimen (B: At POD 30 in group C2). The view of fiberoptic bronchoscopy (C: Fresh trachea, D: Trachea of individuals in group C2 at POD 30, "M" indicates the tracheal membrane). H&E staining for identifying repair site in segments of the cartilage ring. The consecutive photographs of the repaired area in group C2 (E-G: Black arrow indicated the native tracheal epithelium, the yellow arrow is the new epithelial cell layer on the inner surface of the matrix. Magnification: ×40). The appearance of cell strips outside the matrix of group C2 (H: The red arrow indicates, the "C" shape: cartilage rings. Magnification: ×200).

erwise, air leakage would repeatedly occur, and the airway and incision would be infected (**Figure 4A**).

Individuals in group A2 were subjected to allogeneic transplantation. Results showed that the animals had a poor general condition after surgery, due to immune rejection. Moreover, symptoms such as wheezing and cyanosis appeared at POD 3, necessitating timely euthanasia. Individuals in groups B2 and C2 exhibited comparatively good general conditions after surgery, which allowed their specimen to be harvested on time on the 30th day (**Figure 4B**).

Results of fiberoptic bronchoscopy and conventional staining: The airways of animals were firstly analyzed via bronchoscopy, prior to harvesting of specimens. At 30 days, the lumen resisted collapse at the point where the patch was sutured, with no evidence of stenosis and only a small amount of mucus was adherent, compared to the native trachea (**Figure 4C**). The mucosa around the lumen appeared white, possibly due to incomplete blood supply (**Figure 4D**).

The PCL scaffold dissolved during waxing, because it was ester-soluble. H&E staining allowed us to locate the repair site of the blank space between the two segments of the cartilage ring of the harvested tissue at POD 30. A continuous epithelial coverage was also observed at the repair site in group B2 individuals (**Figure 4E-G**: yellow arrow). For those in group C2, the presence of cell strips were considered stem cells, and these were encapsulated in Pluronic F-127 (**Figure 4H**: red arrow). The light-blue development represents surgical sutures.

Immuno-histochemical staining reveals differentiation of epithelial and stem cells: In order to further detect the crawling states of epithelial cells at the repair site, this experiment was performed using CK-18 antibody which was specifically expressed by epithelial cells. The repair

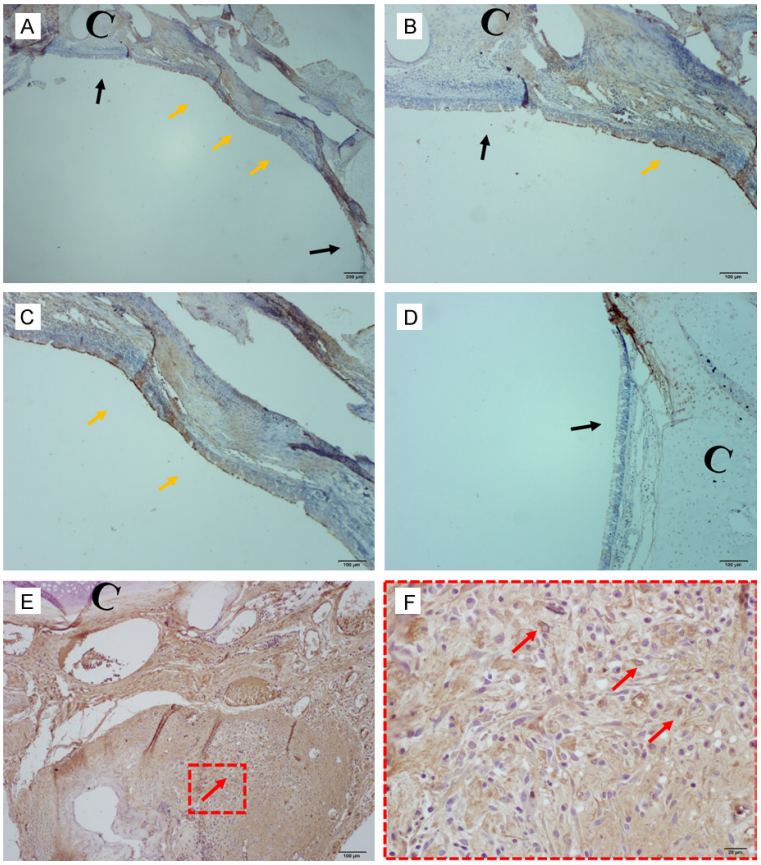

Figure 5. IHC staining of CK-18 consecutive photos of repair sites (yellow arrow) in group C2 (A), partial enlargement of three different areas of (A) (B, C and D, black arrow: the native tracheal epithelium. Magnification: A: ×40, B-D: ×100). The postoperative IHC staining of type-II collagen. (Red arrows: positive cells; "C" shape: cartilage rings. Magnification E: ×100, F: ×400).

sites were covered with continuous brown-colored antigen (**Figure 5A-C**, yellow arrow). Similarly, in order to evaluate whether BMSCs implanted in group C2 could continue to expand and differentiate *in vivo*, IHC staining of type-II collagen antibodies was performed in this experiment. It was found that in the lateral region of the cartilage rings, cell clumps existed (**Figure 5E**) which were stem cells planted on the outer surface of the scaffold during operation. At high magnification, type-II collagen was capable of expressing the cytoplasm of stem cells (**Figure 5F**, indicated by the red arrows).

Long-term efficacy of the 3D scaffold: In group C2, the areas around the anastomosis needed reinforcement treatment after smearing Pluronic F-127 hydrogel on the scaffold (**Figure 6A**). Similarly, the nearby tissues were completely removed in order to avoid loss of the cells on the surface following surgery. To assess the long-term effects of PTS, the observation period was extended for group C2 (POD 90, **Figure 6B**), to allow complete evaluation of the animals' long-term survival condition. Results are summarized in **Table 2**. At POD 90, there was no airway secretion adhering to the patch, and the mucosa had a normal color. However, the lumen was slightly narrow in the expiratory phase (**Figure 6C**). This may possibility be due to an underlying predilection for scarring at surgical sites, although the animals' general health, with regards to weight, respiratory and heart rates, as well as other physiological indices, remained normal. We then analyzed the tissue samples using H&E staining and IHC staining. Results revealed newer glandular tissues and blood vessels between the two cartilage rings (the repair site) compared to those at 30 days (**Figure 6D**, **6E**, red mark). CK-18 staining also revealed presence of a continuous epithelial lining on the inner surface of the lumen (**Figure 6F**, yellow arrow).

Establishment of a rabbit tracheal segmental defect model

Intraoperative anastomosis, postoperative survival rates and specimen harvesting: After the aforementioned surgical operation, the distal airway patency was focused on keeping to prevent the blood clots from slipping into its distal end and avoid postoperative pulmonary complications. At the same time, the tracheal membrane portions and cartilage rings were aligned to avoid tearing and angulation. Besides, the anastomosis site was also carefully checked after suturing (with or without air leakage, exudation, among others), and if necessary, the embedding was intermittently strengthened or covered it with the surrounding muscles and fascias. Healthy conditions after the operation across each group are shown in **Figure 7A-D**.

Animals in groups A3, B3 and C3 did not survive at POD 30 due to postoperative complica-

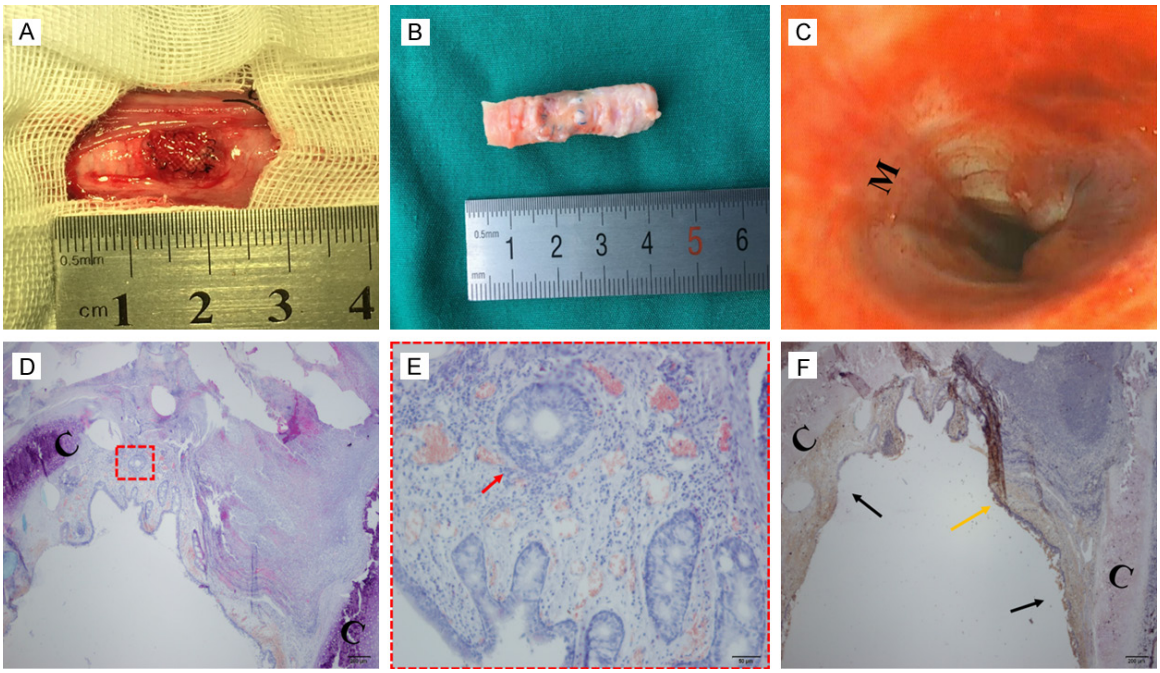

Figure 6. Intraoperative conditions across in group C2 (A: Addition of the gel containing growth factors and stem cells onto the surface). The photograph of harvested specimen (B: At POD 90 in group C2). The view of fiberoptic bronchoscopy (C: Trachea of individuals in group C2 at POD 90, "M" indicates position of the tracheal membrane). HE staining revealed newer blood vessels and glandular tissues between the two cartilage rings (the repair site) compared to those at 30 days (D, E, red mark). CK-18 staining showed that the continuous epithelial cell covered in the lumen (F: yellow arrow, "C" shape: cartilage rings; black arrows indicate the native tracheal epithelium. Magnification: D, F: ×40, E: ×200).

tions. Consequently, general the conditions were monitored, to allow for implementation of timely interventions. The resulting times are outlined in **Table 3**. The postoperative samples of each group were harvested and photographed with photos showing that the cartilage cavity gradually grew bigger in space (**Figure 7E**). Summarily, individuals in group A3 exhibited a lumen that had a serious collapse, followed by those in group B3. Those in group C3 exhibited a porous structure, with complications that occurred at the acute phase.

Microscopic analysis of conventional staining: The harvested tissues were subjected to H&E staining and we observed them under the microscope. Results revealed a large number of inflammatory cells that infiltrated the lumen of individuals in group A3, as evidenced by existence of numerous yellow necrotic tissues (**Figure 7F**). Inflammatory cells on the medial side of individuals in group B3 were fewer than those in group A3, although the mechanical characteristics of the lumens were unstable between these groups. Consequently, the aim of airway-functional replacement in recipients could not be achieved after surgery (**Figure 7G**). Notably, only the surrounding connective tissue from individuals in group C3 could be observed by chemical staining (**Figure 7H**), due to the ester solubility of the PCL scaffold which allows it to dissolve during the waxing. The luminal structure of animals in group D3 was intact, while their epithelial cells crawled on the inner side. In addition, the outer side of their cartilage rings was covered with cord-like fibers (**Figure 7I**).

Epithelial crawling states: The postoperative samples of group D3 were harvested and photographed with photos in **Figure 8A**, **8B**. The lumen of group D3 appeared unobstructed at POD 30, although no signs of stenosis were found, and a small amount of mucus that adhered to the partial tracheal graft. However, mucosa at the transplanted sites turned white, possibly due to incomplete blood supply (**Figure 8C**). Consequently, the observations were continued to be monitored over time. The diameter of the lumen reduced, in rabbits in group D3

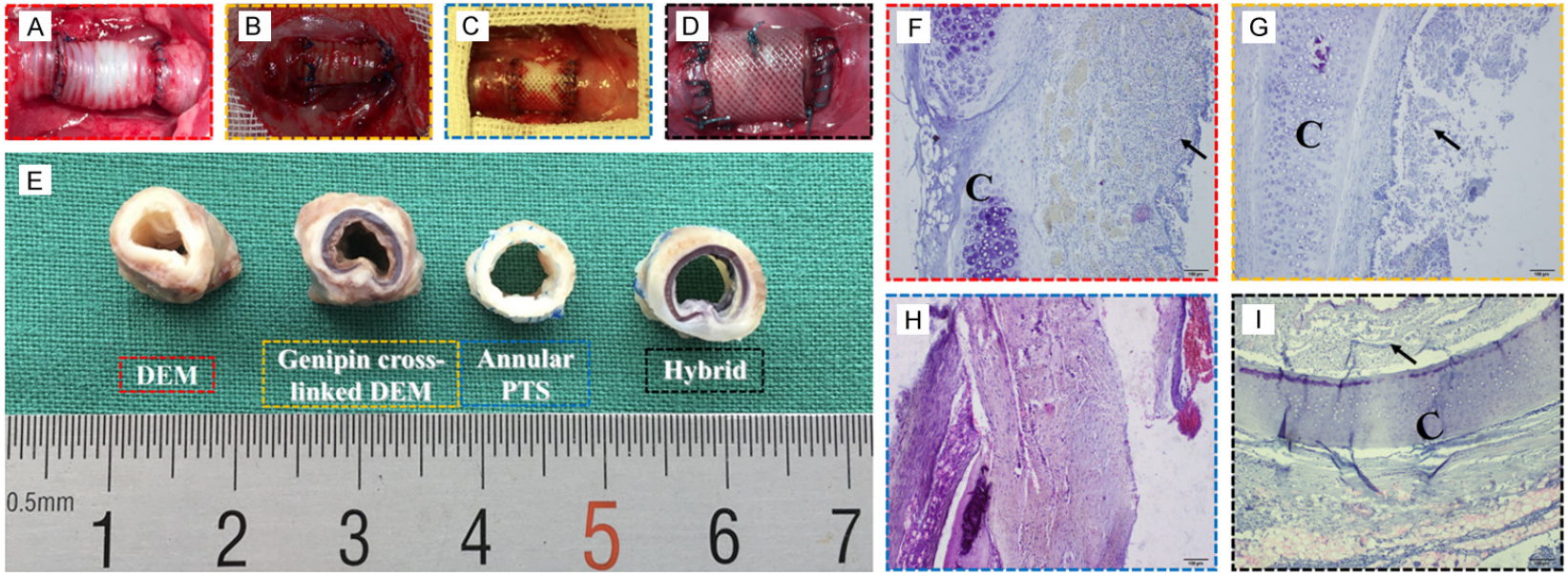

Figure 7. The appearance of tissues during the operation following anastomosis (A: group A3, B: group B3, C: group C3, D: group D3). Post-operative tissue harvesting (E: Bioengineered matrices harvested at the observation time point across the four groups). Postoperative H&E staining (F: group A3, G: group B3, H: group C3, I: group D3. Black arrow indicates the inside lumen, "C" shape: cartilage rings. Magnification: ×100).

Table 2. Profiles of animals' health conditions across each patch-repairing group after surgery

Grouping	Number of animals	Initial weight (kg)	Weight at POD 30 (kg)	Operative anastomosis time (Minutes)	Survival time (Days)	Complications	Prognosis
Native trachea	6	2.87±0.65	-	11.3±2.5	3.13±0.74	Acute rejection	choking
PCL patch only	6	2.92±0.27	3.8±0.23	10.7±1.8	30	none	In good condition
Modified PTS patch+BMSCs	10	3.05±0.28	3.9±0.13	13.7±1.8	30 (4 rabbits were observed over 90 days)	none	In good condition

Table 3. Records of animals' health status across each group after tracheal segmental replacement

Grouping	Number of animals	Initial Weight (kg)	Weight at harvesting (kg)	Operative anastomosis time (Minutes)	Survival time (Days)	Complications	Prognosis
Decellularization	6	2.92±0.27	-	26.3±2.2	13.17±1.47	Lumen collapsed	choking
Genipin+Decellularization	6	2.89±0.46	-	27.1±1.6	18.92±2.31	Lumen collapsed	choking
Tubular PCL scaffold	6	3.01±0.27	-	14.8±1.5	3.67±0.82	Air-leaking and infection	Pustules clogged the airways
Hybrid scaffold	10	3.05±0.28	3.8±0.23	30.7±1.8	30 (4 rabbits were observed for 60 days)	none	In good condition

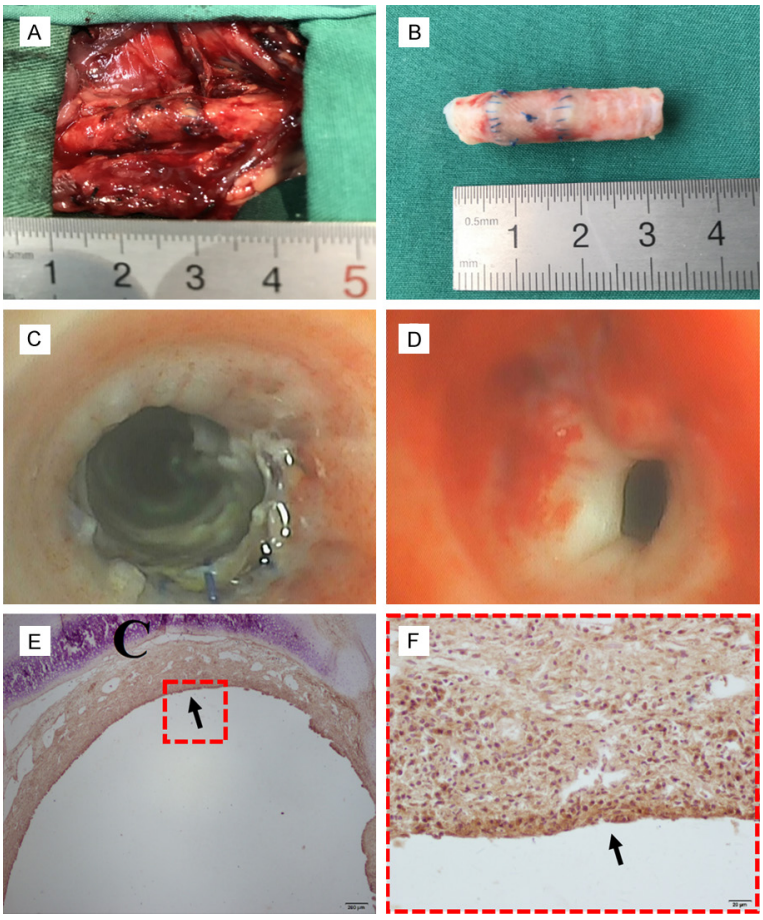

Figure 8. The specimens of group D3 harvested at day 30 (A, B). Profiles of the epithelium's states following fiberoptic bronchoscopy (C: group D3 at 30 days. D: D3 group at 60 days). Postoperative IHC staining of CK-18 (E, F: substitution site in group D3, black arrows indicate the same part inside the lumen. Magnification: C: ×40, D: ×400).

before harvesting and 2 months after surgery. Particularly, no obvious signs of secretion were found and the color of the mucosa appeared slighlty pale. The evidence of existence of local scar hyperplasia was found, which caused the lumen to get narrower during the expiratory phase (**Figure 8D**). However, the experimental animal's body weight did not significantly increase, while wheezing was occasionally observed during breathing. Nevertheless, the animals' general condition was fine. Therefore, future research, aiming to enhance the animals' long-term survival, is advised to implant the epithelium on the inner surface of the matrice. The staining in group D3 individuals at POD 30 was performed, and found continuous epithelial cell coverage on the lumen's inner side (**Figure 8E**, **8F**).

Discussion

Synthetic scaffolds have been associated with various limitations, such as long revascularization periods, difficulty in integration with recipients' tissues, and rejection by the foreign body [10]. These limitations have led to graft's hardening, displacement, and infection after implantation, thereby constraining their long-term efficacy. Since the airway is an organ that communicates with the environment *in vitro*, it needs to be equipped with a certain function of immune clearance. Reconstructing surgery of the trachea not only aims to achieve continuous patency of the lumen, but also guarantees efficient improvement and modification of grafts [11].

Poly-ε-caprolactone, an organic substance polymerized by ε-caprolactone monomer, is non-toxic white solid powder that is insoluble in water but soluble in various organic solvents [12]. The PCL scaffold combines biocompatibility, organic polymerizability and biodegradability, hence can be used as a supportive material for cell growth. In fact, it shows no signs of incompatability with a variety of conventional materials [13]. In addition, PCL also has excellent shape memory and temperature controllability, hence plays an important role in many medical fields, such as preparation of pharmaceutical carriers, degradable organic materials, and nano-spinning materials, among others [14]. Scaffolds made up of PCL, have been widely used in medical devices and tissue engineering. For example, Park's resarch group developed a bellow-like PCL scaffold using 3D printing technology, which has great biomechanical properties such as strong longitudinal regidity and flexibility. Moreover, another study using a rabbit model found that the scaffold coexisted with newborn connective tissues, wi-

thout obstructing the lumen 8 weeks after implantation [15]. Moreover, Ghorbani inoculated BMSCs on a PTS and performed a surgery of rabbit tracheal reconstruction, and observed positive postoperative survival states in the animals [16]. On the other hand, Ott's research team utilized the 3D printing technology to create a scaffold, with a similar structure to the shape of the native tracheal cartilage, and found that the scaffold had excellent mechanical properties [17]. Several other studies have analyzed the scaffold using macroscopic and microscopic geometry [18] and planted different cell lines (such as epithelial cells [19] or chondrocytes [15]) *in vitro* and *in vivo*, and validated the scaffold's biocompatibility. For example, Kaye [20] used a PTS to successfully perform transplantation experiment in a porcine softened trachea model. With regards to clinical application, Les presents the clinical results of 15 patients treated with 3D-printed, patient-specific, externally-implanted, bioresorbable airway splints. The overall device-related complication and mortality rates were low in this population of critically ill, medically-complex patients [21]. Similarly, Morrison demonstrated successful treatment of life-threatening acquired tracheomalacia with a 3D printed bio-permanent tracheal splint in a 14-year-old female patient for whom all prior therapeutic approaches had failed [22]. Furthermore, Arcieri reported the use of 3D printing technology after an unsuccessful surgical treatment on a 6-year-old boy diagnosed to have congenital tracheal stenosis associated to pulmonary sling [23]. Taken together, results from these experimental studies and related reports of clinical success indicate that scaffolds made up of PTS hold great promise for airway reconstruction. Rapid development of 3D bio-printing technology is expected to enhance generation of bio-composites for future tissue engineering.

Despite these successes, the hydrophobic structure on the surface of PCL scaffold has been shown to affect cells' anchoring ability, thereby constraining the associated biological activities such as cells' growth and migration [24]. In order to circumvent the shortcomings associated with this structure, researchers have attempted various approaches, such as making use of collagen, gelatin or combining vascular growth factors and other protein components. Others have adopted use of other chemical technologies, such as polymer materials and UV ozone, to enhance the scaffolds' surface properties [25, 26]. Results from the above studies indicate that surface-modification technology can effectively improve the cytoplasmicity of the scaffold without depriving it of its original biological properties. Consequently, these studies lay a theoretical basis for future application of this approach. In the present study, The PTS was modified via 20% Pluronic F-127 and co-cultured them with stem cells *in vitro*. Our results show that scaffold has excellent biocompatibility hence promising for future application.

In recent years, several studies have investigated whether a cell-scaffold complex can be used in *in situ* transplantation following cultivating an *in vivo* bioreactor, and found promising results at both experimental and clinical levels [27]. Currently, many research groups have advocated for the use of a body's internal environment as a "dynamic bioreactor". This concept circumvents the need for *in vitro* expansion prior to their implantation on the graft. This is practical for future clinical applications, especially for those who urgently need alternative treatment on account of saving operating costs and time [27-29]. Theoretically, the natural microenvironment around a recipient's transplanted site transmits repair signals by releasing relevant growth factors, which promote autologous stem cells' graft-enabled migration and differentiation, thus making a leap towards the regeneration of tissue engineering grafts [30]. In the present study, two different animal models were successfully designed, one for partial tracheal window-shape and the other for tracheal segmental defect repairment, based on previous studies. Postoperative observations revealed normal health conditions in the recipients. At 30 days, the lumen appeared smooth and there was evidence of epithelial cell crawling on the replaced patch. Implanted BMSCs successfully differentiated into chondrocytes in the hydrogel carrier rich in growth factors, thanks to the natural environment of the human body.

The natural matrix needs to meet some requirements for a suitable tracheal graft. Although initial studies showed that decellularization does not significantly affect the trachea's bio-

mechanical properties [31, 32], subsequent investigations have demonstrated that a scaffold's ability to resist radial compressive strength worsens during this process. Consequently, the tracheal lumen is likely to undergo varying degrees of collapse after operation, thereby exerting negative effects on the clinical practice, especially with respect to the long-term efficacy [33]. Rapid development of 3D printing technology has enhanced its performance across tissue engineering as well as many other fields [34]. Taken together, the findings of this study have significant implications in improving stability of the graft's structure and reducing incidence of lumen collapse after transplantation. For an optimal PTS for construction of adequate tracheal substitutes, various precautions need to be considered. For example, it ensured that the microstructure was adequately improved, and its biocompatibility indicators, such as cells' attachment, growth and proliferation states were appropriately assessed. Secondly, it organically combined natural scaffolds (decellularized matrix cross-linked with genipin). Overall, the findings of this study lay a theoretical foundation for the clinical application of tissue-engineered tracheal transplantation. Harvesting of the hybrid tracheal graft prepared in our study, at POD 60, revealed that the lumen exhibited partial stenosis under the fiberoptic bronchoscope (especially in the expiratory phase), while the recipients' general condition was good. Despite these breakthroughs, further research is needed to enlarge the sample capacity and prolong the observation time. It is also necessary to implant autologous epithelium or stem cells, which have been induced to differentiate into epithelial cells on the inner surface of the scaffold. Finally, further improvement of stenosis symptoms is imperative to promoting the the long-term survival condition of the recipients.

Conclusions

The modified PTS with 20% Pluronic F-127 has excellent biocompatibility. We combined a 3D printing porous tracheal patch with a hydrogel carrier rich in BMSCs and growth factors to successfully establish a rabbit model for tracheal partial window-shape defect repair. A tracheal substitute hybridized with modified 3D printing porous "C"-shaped outer scaffold and decellularized matrix successfully established a rabbit tracheal segmental defect model.

Acknowledgements

This study was supported by the National Natural Science Foundation of China (Grant No. 82070020), the Natural Science Foundation for the Youth of Jiangsu Province (No. BK20200196), the Research Project of Gusu Health Talents in Suzhou (No. GSWS2021013) and the Postgraduate Research & Practice Innovation Program of Jiangsu Province (No. SJXC21_1352).

Disclosure of conflict of interest

None.

Address correspondence to: Hongcan Shi, Clinical Medical College, Yangzhou University, No. 136, Jiangyang Middle Road, Hanjiang District, Yangzhou 225000, Jiangsu, China. Tel: +86-18051062168; Fax: 0514-87978801; E-mail: shihongcan@yzu.edu.cn

References

[1] Simitzi C, Vlahovic M, Georgiou A, Keskin-Erdogan Z, Miller J and Day RM. Modular orthopaedic tissue engineering with implantable microcarriers and canine adipose-derived mesenchymal stromal cells. Front Bioeng Biotechnol 2020; 8: 816.

[2] Vranckx JJ and Delaere P. The current status and outlook of trachea transplantation. Curr Opin Organ Transplant 2020; 25: 601-608.

[3] Fan D, Li Y, Wang X, Zhu T, Wang Q, Cai H, Li W, Tian Y and Liu Z. Progressive 3D printing technology and its application in medical materials. Front Pharmacol 2020; 11: 122.

[4] Ohno M, Fuchimoto Y, Higuchi M, Yamaoka T, Komura M, Umezawa A, Hsu HC, Enosawa S and Kuroda T. Long-term observation of airway reconstruction using decellularized tracheal allografts in micro-miniature pigs at growing stage. Regen Ther 2020; 15: 64-69.

[5] Batioglu-Karaaltin A, Ovali E, Karaaltin MV, Yener M, Yilmaz M, Eyupoglu F, Yilmaz YZ, Bozkurt ER, Demir N, Konuk E, Bozdag ES, Yigit O and Cansiz H. Decellularization of trachea with combined techniques for tissue-engineered trachea transplantation. Clin Exp Otorhinolaryngol 2019; 12: 86-94.

[6] Park JH, Park JY, Nam IC, Ahn M, Lee JY, Choi SH, Kim SW and Cho DW. A rational tissue engineering strategy based on three-dimensional (3D) printing for extensive circumferential tracheal reconstruction. Biomaterials 2018; 185: 276-283.

[7] Wang Z, Sun F, Lu Y, Pan S, Yang W, Zhang G, Ma J and Shi H. Rapid preparation of decellu-

larized trachea as a 3D scaffold for organ engineering. Int J Artif Organs 2021; 44: 55-64.
[8] Su D, Tsai HI, Xu Z, Yan F, Wu Y, Xiao Y, Liu X, Wu Y, Parvanian S, Zhu W, Eriksson JE, Wang D, Zhu H, Chen H and Cheng F. Exosomal PD-L1 functions as an immunosuppressant to promote wound healing. J Extracell Vesicles 2019; 9: 1709262.
[9] Zhong Y, Jiang A, Sun F, Xiao Y, Gu Y, Wu L, Zhang Y and Shi H. A comparative study of the effects of different decellularization methods and genipin-cross-linking on the properties of tracheal matrices. Tissue Eng Regen Med 2019; 16: 39-50.
[10] Baptista R and Guedes M. Morphological and mechanical characterization of 3D printed PLA scaffolds with controlled porosity for trabecular bone tissue replacement. Mater Sci Eng C Mater Biol Appl 2021; 118: 111528.
[11] Dikina AD, Alt DS, Herberg S, McMillan A, Strobel HA, Zheng Z, Cao M, Lai BP, Jeon O, Petsinger VI, Cotton CU, Rolle MW and Alsberg E. A modular strategy to engineer complex tissues and organs. Adv Sci (Weinh) 2018; 5: 1700402.
[12] Kambhampati SBS and Vaishya R. Publication trends of PCL in the last 40 years on PubMed. J Clin Orthop Trauma 2020; 11 Suppl 3: S354-S361.
[13] Chan DS, Gabra N, Baig A, Manoukian JJ and Daniel SJ. Bridging the gap: using 3D printed polycaprolactone implants to reconstruct circumferential tracheal defects in rabbits. Laryngoscope 2020; 130: E767-E772.
[14] Park JH, Yoon JK, Lee JB, Shin YM, Lee KW, Bae SW, Lee J, Yu J, Jung CR, Youn YN, Kim HY and Kim DH. Experimental tracheal replacement using 3-dimensional bioprinted artificial trachea with autologous epithelial cells and chondrocytes. Sci Rep 2019; 9: 2103.
[15] Lee JY, Park JH and Cho DW. Comparison of tracheal reconstruction with allograft, fresh xenograft and artificial trachea scaffold in a rabbit model. J Artif Organs 2018; 21: 325-331.
[16] Ghorbani F, Moradi L, Shadmehr MB, Bonakdar S, Droodinia A and Safshekan F. In-vivo characterization of a 3D hybrid scaffold based on PCL/decellularized aorta for tracheal tissue engineering. Mater Sci Eng C Mater Biol Appl 2017; 81: 74-83.
[17] Yu YS, Ahn CB, Son KH and Lee JW. Motility improvement of biomimetic trachea scaffold via hybrid 3d-bioprinting technology. Polymers (Basel) 2021; 13: 971.
[18] Jung H, Lee JS, Lee JH, Park KJ, Lee JJ and Park HS. A feasibility study for 3d-printed poly(methyl methacrylate)-resin tracheostomy tube using a hamster cheek pouch model. In Vivo 2020; 34: 1749-1758.
[19] Machino R, Matsumoto K, Taniguchi D, Tsuchiya T, Takeoka Y, Taura Y, Moriyama M, Tetsuo T, Oyama S, Takagi K, Miyazaki T, Hatachi G, Doi R, Shimoyama K, Matsuo N, Yamasaki N, Nakayama K and Nagayasu T. Replacement of rat tracheas by layered, trachea-like, scaffold-free structures of human cells using a bio-3D printing system. Adv Healthc Mater 2019; 8: e1800983.
[20] Kaye R, Goldstein T, Aronowitz D, Grande DA, Zeltsman D and Smith LP. Ex vivo tracheomalacia model with 3D-printed external tracheal splint. Laryngoscope 2017; 127: 950-955.
[21] Les AS, Ohye RG, Filbrun AG, Ghadimi Mahani M, Flanagan CL, Daniels RC, Kidwell KM, Zopf DA, Hollister SJ and Green GE. 3D-printed, externally-implanted, bioresorbable airway splints for severe tracheobronchomalacia. Laryngoscope 2019; 129: 1763-1771.
[22] Morrison RJ, Sengupta S, Flanangan CL, Ohye RG, Hollister SJ and Green GE. Treatment of severe acquired tracheomalacia with a patient-specific, 3D-printed, permanent tracheal splint. JAMA Otolaryngol Head Neck Surg 2017; 143: 523-525.
[23] Arcieri L, Giordano R, Bellanti E, Chiappino D and Murzi B. Impact of 3D printing on the surgical management of tracheal stenosis associated to pulmonary sling: a case report. J Thorac Dis 2018; 10: E130-E133.
[24] Pan S, Zhong Y, Shan Y, Liu X, Xiao Y and Shi H. Selection of the optimum 3D-printed pore and the surface modification techniques for tissue engineering tracheal scaffold in vivo reconstruction. J Biomed Mater Res A 2019; 107: 360-370.
[25] Wasyleczko M, Sikorska W and Chwojnowski A. Review of synthetic and hybrid scaffolds in cartilage tissue engineering. Membranes (Basel) 2020; 10: 348.
[26] Hwang TI, Lee SY, Lee DH, Park JK, Park CH and Kim CS. Fabrication of bioabsorbable polylactic-co-glycolic acid/polycaprolactone nanofiber coated stent and investigation of biodegradability in porcine animal model. J Nanosci Nanotechnol 2020; 20: 5360-5364.
[27] Hamilton NJI, Hynds RE, Gowers KHC, Tait A, Butler CR, Hopper C, Burns AJ, Birchall MA, Lowdell M and Janes SM. Using a three-dimensional collagen matrix to deliver respiratory progenitor cells to decellularized trachea in vivo. Tissue Eng Part C Methods 2019; 25: 93-102.
[28] Park HS, Lee JS, Jung H, Kim DY, Kim SW, Sultan MT and Park CH. An omentum-cultured 3D-printed artificial trachea: in vivo bioreactor. Artif Cells Nanomed Biotechnol 2018; 46 Suppl 3: S1131-S1140.

[29] Hatachi G, Matsumoto K, Miyazaki T, Tsuchiya T, Taniguchi D, Doi R, Watanabe H, Nakatsukasa T, Matsuo N and Nagayasu T. Enhanced airway stenting using a preoperative, three-dimensionally printed airway model simulation. Gen Thorac Cardiovasc Surg 2020; 68: 1591-1593.

[30] Gilevich IV, Sotnichenko AS, Karal-Ogly DD, Gubareva EA, Kuevda EV, Polyakov IS, Lapin BA, Orlov SV, Porkhanov VA and Chekhonin VP. In vivo experimental study of biological compatibility of tissue engineered tracheal construct in laboratory primates. Bull Exp Biol Med 2018; 164: 770-774.

[31] Dimou Z, Michalopoulos E, Katsimpoulas M, Dimitroulis D, Kouraklis G, Stavropoulos-Giokas C and Tomos P. Evaluation of a decellularization protocol for the development of a decellularized tracheal scaffold. Anticancer Res 2019; 39: 145-150.

[32] Hong P, Bezuhly M, Graham ME and Gratzer PF. Efficient decellularization of rabbit trachea to generate a tissue engineering scaffold biomatrix. Int J Pediatr Otorhinolaryngol 2018; 112: 67-74.

[33] Deslauriers J, Aubree N and Shamji FM. Experiences with prosthetic airway replacement. Thorac Surg Clin 2018; 28: 377-384.

[34] Pennarossa G, Arcuri S, De Iorio T, Gandolfi F and Brevini TAL. Current advances in 3D tissue and organ reconstruction. Int J Mol Sci 2021; 22: 830.